MOEM

Modern Electronic Materials 2023; 9(2): 69–76
DOI 10.3897/j.moem.9.2.109743

Research Article

Comparison between optical and electrical data on hole concentration in zinc-doped *p*-GaAs

Aleksandr G. Belov[1], Vladimir E. Kanevskii[1], Evgeniya I. Kladova[1], Stanislav N. Knyazev[1], Nikita Yu. Komarovskiy[1,2], Irina B. Parfent'eva[1], Evgeniya V. Chernyshova[1,2]

1 Federal State Research and Development Institute of Rare Metal Industry (Giredmet JSC), 2-1 Elektrodnaya Str., Moscow 111524, Russian Federation

2 National University of Science and Technology "MISIS", 4-1 Leninsky Ave., Moscow 119049, Russian Federation

Corresponding author: Aleksandr G. Belov (b9151609271@gmail.com)

Received 13 April 2023 ♦ **Accepted** 19 June 2023 ♦ **Published** 5 July 2023

Citation: Belov AG, Kanevskii VE, Kladova EI, Knyazev SN, Komarovskiy NYu, Parfent'eva IB, Chernyshova EV (2023) Comparison between optical and electrical data on hole concentration in zinc-doped *p*-GaAs. *Modern Electronic Materials* 9(2): 69–76. https://doi.org/10.3897/j.moem.9.2.109743

Abstract

The optical and electrical properties of zinc-doped Cz *p*-GaAs have been studied. Reflection spectra of ten *p*-GaAs specimens have been taken in the mid-IR region. Van der Pau galvanomagnetic, electrical resistivity and Hall coefficient measurements have been carried out for the same specimens (all the measurements were carried out at room temperature). The reflection spectra have been processed using the Kramers–Kronig relations, spectral dependences of the real and imaginary parts of the complex dielectric permeability have been calculated and loss function curves have been plotted. The loss function maximum position has been used to calculate the characteristic wavenumber corresponding to the high-frequency plasmon-phonon mode frequency. Theoretical calculations have been conducted and a calibration curve has been built up for determining heavy hole concentration in *p*-GaAs at $T = 295$ K based on known characteristic wavenumber. Further matching of the optical and Hall data has been used for determining the light to heavy hole mobility ratio. This ratio proves to be in the 1.9–2.8 range which is far lower as compared with theoretical predictions in the assumption of the same scattering mechanism for light and heavy holes (at optical phonons). It has been hypothesized that the scattering mechanisms for light and heavy holes differ.

Keywords

gallium arsenide, electron concentration, Hall effect, reflection spectrum, plasmon-phonon interaction

1. Introduction

This paper is a continuation of our earlier works at Giredmet JSC aimed at developing a contactless non-destructive optical method of free carrier concentration measurement in heavily doped semiconductors. The basic principle of the method is as follows. A reflection spectrum is taken from the test specimen in the mid-IR region. The reflection spectrum is analyzed using the Kramers–Kronig relations in order to determine the characteristic wavenumber based on which the free carrier concentration (FCC) is calculated.

This approach has a number of advantages over the conventional Hall method: it does not require attaching contacts to the specimen and is streamlined and local (the probing area depends on the light spot dimensions). Furthermore, by moving the specimen relative to the light spot one can take reflection spectra at different points on the test specimen and thus to have an overview of the FCC distribution over its area.

The required calculations were made for n-InSb [1], n-GaAs [2], n-InAs [3] at $T = 295$ K. For the same specimens, galvanomagnetic measurements were carried out along with optical ones [2, 3], and the results yielded by different methods were compared. However, all these measurements were made for n-type conductivity materials.

In this work we attempted to apply the above described approach to a p-type conductivity material. We studied zinc-doped p-GaAs specimens. Since this material has two types of holes (light and heavy), the earlier approach required a substantial correction, and that is what this work deals with. All the measurements were carried out at room temperature.

The aim of the work was to build up a calibration curve for determining the heavy hole concentration in p-GaAs based on the characteristic wavenumber, carry out optical measurements, calculate the heavy hole concentration and compare the data with electrical measurement data obtained for the same specimens.

2. Specimens and methods

The test materials were zinc-doped single crystal Cz GaAs ingots. (100) oriented wafers were cut from the ingots perpendicular to the growth axis. The wafers were cut into specimens sized 6–10 with the thickness d = 1–2 mm. After cutting the flat specimen surfaces were mechanically ground and then chemomechanicaly polished.

The free carrier concentration was measured by analyzing the mid-IR region reflection spectra of the specimens $R(\nu)$ recorded with a Tensor-27 Fourier spectrometer in the $\nu = 340÷2000$ cm^{-1} wavenumber range with a 2 cm^{-1} resolution. The light spot diameter was 4.5 mm. The reflection spectra were processed using the Kramers–Kronig relations in order to calculate the real ε_1 and imaginary ε_2 parts of the complex dielectric permeability $\varepsilon = \varepsilon_1 + i\varepsilon_2$ as a function of wavenumber and to plot the so-called loss function:

$$\mathrm{LF} = \mathrm{Im}\left(-\frac{1}{\varepsilon}\right) = \frac{\varepsilon_2}{\varepsilon_1^2 + \varepsilon_2^2}.$$

This function has a typical bell-shaped pattern with its maximum corresponding to the characteristic wavenumber. Then this wavenumber was used for calculating the FCC with a special calculation formula taking into account the effect of plasmon-phonon interaction.

The optical data were compared with the electrical measurement results. n-type conductivity materials were studied in earlier works [2, 3], and the electron concentrations obtained with optical methods were matched with the Hall data. This approach, however, is not applicable for a p-type conductivity material since the presence of two types of holes does not allow their specific concentrations to be derived from Hall data (see below for details).

For electrical measurements the contacts were tin-soldered to the edges of specimen butt-ends. Two specimens were placed on a two-side holder one at each side, and the contact wires were soldered to the matching contact pads of the holder. The holder with the specimens was placed in the gap between the poles of an electric magnet core perpendicular to the magnetic field induction vector. The measurements were carried out using a standard four-probe setup (the Van der Pau method). The electrical resistivity was measured without magnetic field, and the Hall coefficient, in a $B = 0.5$ T field with a 200 mA current through the specimen.

3. Theoretical calculations

It is well-known (see e.g. overview [4]) that the valence band of GaAs contains two subbands degenerated at the point Γ of the Brillouin zone (Fig. 1).

In other words, p-type conductivity GaAs contains two types of holes: light and heavy, and hence treatise of optical and electrical measurement data is much complicated as compared with an n-type material which contains only electrons. The plasma frequency ω_p formula for the case of two types of holes is as follows [5]:

$$\omega_p^2 = \frac{4\pi e^2}{\varepsilon_\infty}\left(\frac{p_\mathrm{h}}{m_{p_\mathrm{h}}} + \frac{p_\mathrm{l}}{m_{p_\mathrm{l}}}\right) = \frac{4\pi e^2 p_\mathrm{h}}{\varepsilon_\infty m_{p_\mathrm{h}}}\left(1 + \frac{p_\mathrm{l} m_{p_\mathrm{h}}}{p_\mathrm{h} m_{p_\mathrm{l}}}\right). \quad (1)$$

Here p_h and p_l are the heavy and light hole concentrations, respectively, m_{p_h} and m_{p_l} are their effective optical masses, respectively, ε_∞ is the high-frequency dielectric permeability, $e = 4.8 \cdot 10^{-10}$ CGS u. is the electron charge.

The concentrations of heavy and light holes obey the following relationship:

$$p_\mathrm{h} = \frac{8\pi}{3h^3}\left(2m_{p_\mathrm{h}}kT\right)^{3/2} F_{3/2}(\eta); \quad (2)$$

$$p_\mathrm{l} = \frac{8\pi}{3h^3}\left(2m_{p_\mathrm{l}}kT\right)^{3/2} F_{3/2}(\eta). \quad (3)$$

Here $h = 6.62 \cdot 10^{-27}$ erg·s is Planck's constant, $k = 1.38 \cdot 10^{-16}$ erg/K is the Boltzmann constant (for $T = 295$ K, $kT = 25.4$ meV) and $F_{3/2}(\eta)$ is the one-parameter Fermi integral:

$$F_{3/2}(\eta) = \int_0^\infty \left(-\frac{\partial f_0}{\partial x}\right) x^{3/2} \mathrm{d}x, \quad (4)$$

where $f_0(x, \eta) = [1 + \exp(x - \eta)^{-1}$; $\eta = E_\mathrm{F}/kT$ is the reduced Fermi level (counted down from the valence band ceiling at the Γ-point).

It can be seen from Eqs. (2) and (3) that the heavy to light hole concentration ratio does not depend on the

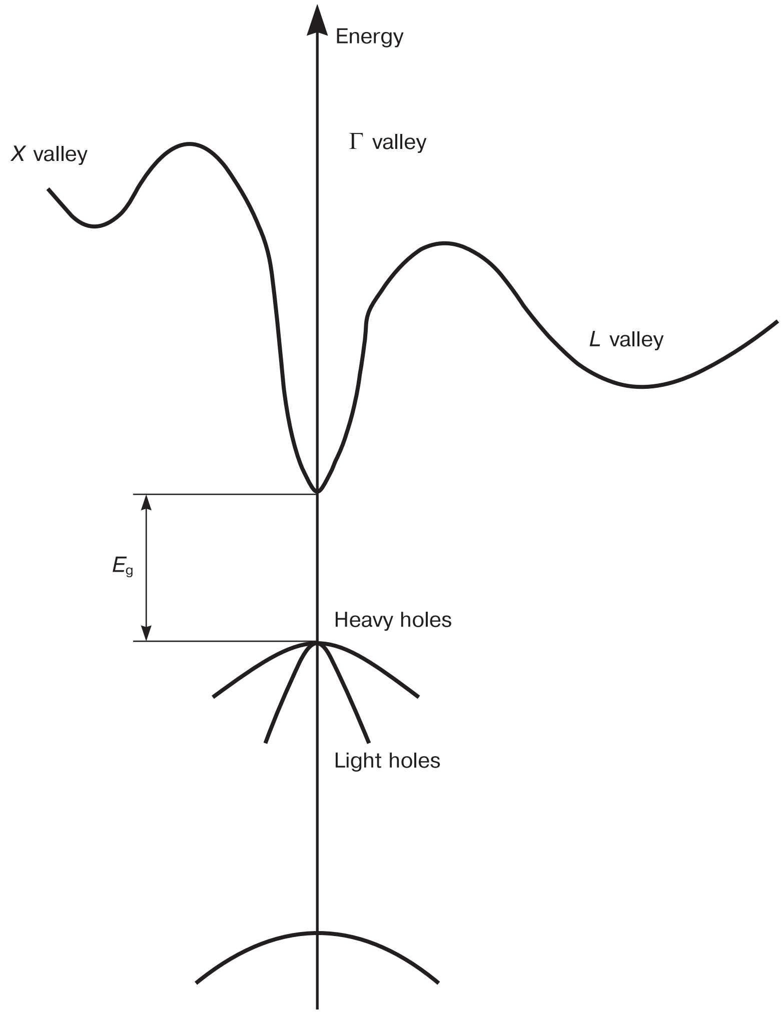

Figure 1. GaAs band structure [4]

reduced Fermi level and equals the heavy to light hole effective mass ratio to a power of 3/2:

$$\frac{p_{\mathrm{h}}}{p_{\mathrm{l}}} = \left(\frac{m_{p_{\mathrm{h}}}}{m_{p_{\mathrm{l}}}}\right)^{3/2}. \qquad (5)$$

It should also be noted that since the heavy and light hole subbands have parabolic shapes and are isotropic, the effective masses of the density of states in Eqs. (2) and (3) equal the effective optical masses in Eq. (1).

Since gallium arsenide is a semiconductor with a substantial fraction of ionic bond, one should take into account the interaction between plasmon oscillations and longitudinal optical phonons (the so-called plasmon-phonon interaction).

In other words, the test material contains not purely plasma oscillations but some combined plasmon-phonon modes [7, 8]. The effect of plasmon-phonon interaction should also be taken into account in studies of the optical properties of other materials [9–14].

In the case in question, neglect of plasmon-phonon interaction can cause a tangible systematic error in FCC measurement.

To calculate the frequencies of the combined plasmon-phonon modes, we use the following relationship:

$$\varepsilon(\omega) = \varepsilon_\infty\left[1-\left(\frac{\omega_p}{\omega}\right)^2\right] + \left(\varepsilon_0-\varepsilon_\infty\right)\left[1-\frac{\varepsilon_0}{\varepsilon_\infty}\left(\frac{\omega}{\omega_{\mathrm{LO}}}\right)^2\right]^{-1}, \qquad (6)$$

where ε_0 is the static dielectric permeability and ω_{LO} is the longitudinal optical phonon frequency. Equation (6) does not take into account the extinction of plasmons and longitudinal optical phonons and therefore the dielectric permeability is not a complex but a natural function of the frequency ω. This approximation is very rough but it provides the desired result.

It is well-known that longitudinal oscillations (and that is what the combined plasmon-phonon modes are) can exist in a media only if its dielectric permeability falls down to zero. Bringing Eq. (6) to zero, solving the biquadratic equation for the frequency of the combined modes ω_- (the low-frequency one) and ω_+ (the high-frequency

Table 1. Calculation results for p-GaAs ($T = 295$ K)

η	$F_{3/2}(\eta)$	p_h (10^{18} cm^{-3})	ν_p (cm^{-1})	ν_+ (cm^{-1})
–1	0.436	2.918	256.6	325.8
–0.5	0.675	4.518	319.2	361.8
0	1.017	6.811	392.0	419.3
0.5	1.485	9.946	473.7	492.9
1	2.095	14.025	562.5	577.2
1.5	2.851	19.092	656.3	668.1
2	3.754	25.135	753.0	762.9
2.5	4.795	32.107	851.1	859.6
3	5.966	39.945	949.3	956.8

one) and transiting from frequencies ω to wavenumbers ν we obtain the following expression:

$$\nu_{\pm}^2 = \frac{1}{2}\left[\left(\nu_p^2 + \nu_{\mathrm{LO}}^2\right) \pm \pm \sqrt{\left(\nu_p^2 + \nu_{\mathrm{LO}}^2\right)^2 - 4\frac{\varepsilon_\infty}{\varepsilon_0}\nu_p^2\nu_{\mathrm{LO}}^2}\right]. \quad (7)$$

We will hereinafter deal only with the high-frequency mode ν_+.

The calculation algorithm is as follows:

– set the value of η and calculate p_h and p_l using Eqs. (2) and (3);

– substitute the result into Eq. (1) and calculate ω_p;

– substitute the result into Eq. (7) and calculate ν_+;

– change the value of η and repeat the above operations;

– build up a calibration curve of heavy hole concentration as a function of characteristic wavenumber $p_h = f(\nu_+)$.

The calculations were carried out with the following parameters borrowed from earlier review [4]: $m_{p_h} = 0.51m_0$; $m_{p_l} = 0.082m_0$; $\varepsilon_0 = 12.9$; $\varepsilon_\infty = 10.9$; $\nu_{\mathrm{LO}} = 291$ cm^{-1} (36.1 meV); $m_0 = 9.11 \cdot 10^{-28}$ g is the free electron mass. Then, in accordance with Eq. (5), the ratio $p_h/p_l = 15.51$. Thus, the second term in the right-hand side of Eq. (1) is 0.4014 and the value in parentheses is 1.4014.

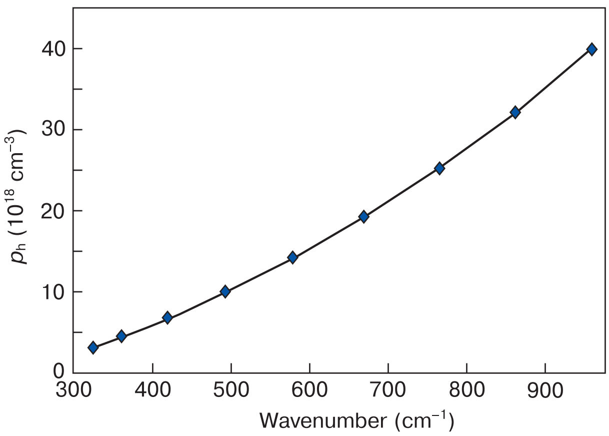

Figure. 2. Calculated calibration curve for heavy hole concentration as a function of characteristic wavenumber

Then Eqs. (2) and (3) take on as follows:

$$p_h = 6.696 \cdot 10^{18} F_{3/2}(\eta); \quad (8)$$

$$p_l = 4.322 \cdot 10^{17} F_{3/2}(\eta). \quad (9)$$

Transiting to wavenumbers one can transform Eq. (1) as follows:

$$\nu_p = 15.02 \cdot 10^{-8}\sqrt{p_h}. \quad (10)$$

Table 1 summarizes the calculation data for heavy hole concentration and the wavenumbers corresponding to the plasma frequency ν_p and the high-frequency plasmon-phonon mode frequency ν_+ for a reduced Fermi level of $-1 \le \eta \le 3$.

As can be seen from Table 1, the difference between ν_p and ν_+ for the same p_h is tangible for $\eta = -1$ and decreases with an increase in η. Thus, the effect of plasmon-phonon interaction decreases with an increase in the hole concentration.

The data presented in Table 1 can be used for building up a calibration curve allowing one to calculate the heavy hole concentration p_h based on the experimentally measured characteristic wavenumber ν_+. This curve is shown in Fig. 2. It can be well described by a second-order polynomial:

$$p_h = 3.937 \cdot 10^{13}(\nu_+)^2 + 7.635 \cdot 10^{15}(\nu_+) - - 3.495 \cdot 10^{18}. \quad (11)$$

If there are two types of holes the Hall coefficient R_H and the electrical resistivity r can be described with the following relationships:

$$R_H = \frac{1}{e}\frac{\left(p_l\mu_{p_l}^2 + p_h\mu_{p_h}^2\right)}{\left(p_l\mu_{p_l} + p_h\mu_{p_h}\right)^2}; \quad (12)$$

$$\rho^{-1} = e\left(p_l\mu_{p_l} + p_h\mu_{p_h}\right). \quad (13)$$

Introducing the dimensionless parameter equalling the light to heavy hole mobility ratio $b = \mu_{p_l}/\mu_{p_h}$, one can transform Eqs. (12) and (13) as follows:

$$R_H = \frac{1}{e}\frac{\left(p_l b^2 + p_h\right)}{\left(p_l b + p_h\right)^2}; \quad (14)$$

$$\rho^{-1} = e\mu_{p_h}\left(p_l b + p_h\right). \quad (15)$$

Taking into account that p_h = 15.51p_l, we finally obtain:

$$R_H = \frac{1}{ep_h}\frac{(1+0.06447b^2)}{(1+0.06447b)^2}; \quad (16)$$

$$\rho^{-1} = e\mu_{p_h} p_h(1+0.06447b). \quad (17)$$

Thus, having determined p_h from optical data using the calibration function as per Eq. (11) and knowing R_H, one can use Eq. (16) to calculate the parameter b and then use Eq. (17) to calculate μ_{p_h} based on known ρ. To the best of our knowledge, this approach is used for the first time.

4. Results and discussion

A typical room temperature reflection spectrum of zinc-doped *p*-GaAs specimens is shown in Fig. 3, *a* (Curve *1*, Specimen *9*, see Table 2). Also shown is the loss function whose y axis scale was increased 10-fold for the sake of visibility (Curve *2*). To demonstrate the difference between the reflection spectra of the *n*- and *p*-type conductivity specimens, Fig. 3 *b* shows the reflection spectrum of an *n*-type GaAs specimen with the electron concentration $n = 9.9 \cdot 10^{17}$ cm^{-3} (Curve *1*) and the loss function for this spectrum (Curve *2*, *y* axis scale is the same).

The minimum in the reflection spectrum of the *p*-type specimen (Fig. 3 *a*, Curve *1*) is far less pronounced than that of the *n*-type specimen (Fig. 3 *b*, Curve *1*). Thus, the loss function curve for the *p*-type specimen (Fig. 3 *a*, Curve *2*) is far more smeared than that for the *n*-type specimen (Fig. 3 *b*, Curve *2*). Note that the loss function minima for both specimens are shifted relative to the reflection spectrum minima towards smaller wavenumbers.

Reflection spectrum pattern is known to depend on reflecting surface treatment quality. We specially studied

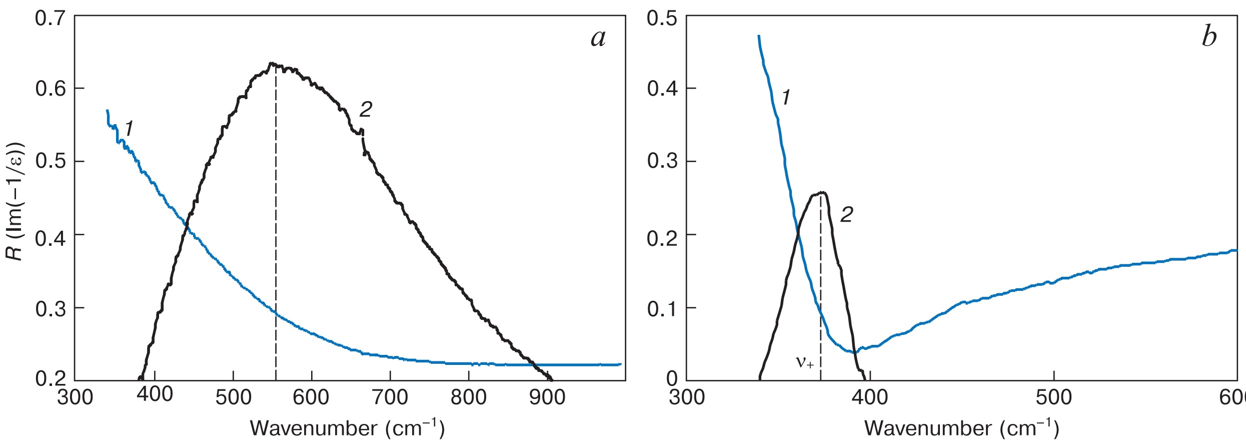

Figure. 3. (*1*) reflection spectra and (*2*) loss function curves for (*a*) *p*-type and (*b*) *n*-type GaAs specimens

Table 2. Parameters of test specimens

Specimen	d (mm)	ρ (Ohm · cm)	R_H (cm^3/Cl)	ν_+ (cm^{-1})	p_h (10^{18} cm^{-3})	b	μ_{p_h} (cm^2/(V · s))
1	1.87	0.015	+1.5	359	4.32	2.5	90
2	1.66	0.013	+1.4	374	4.87	2.8	80
3	1.36	0.012	+1.12	395	5.66	2.7	80
4	1.33	0.010	+0.91	420	6.66	1.9	80
5	1.09	0.010	+0.93	429	7.03	2.5	80
6	1.55	0.0090	+0.80	444	7.66	1.9	80
7	1.64	0.0091	+0.80	456	8.17	2.5	70
8	1.72	0.0080	+0.66	488	9.61	2.3	70
9	1.28	0.0063	+0.50	551	12.7	2.2	80
10	1.36	0.0056	+0.39	615	16.1	2.3	60

earlier [3] how surface roughness affects the spectral function $R(\nu)$ of n-InAs specimens. We first took reflection spectra from a polished surface and then treated the reflecting surfaces with a 10 μm grinding powder to make them matt. The study showed that the reflection spectrum minimum became less pronounced after grinding and the loss function curve was broadened while decreasing in magnitude.

However this explanation is not applicable to the case considered since the reflecting surfaces of the n- and p-type GaAs specimens were similar. It is safe to assume that the difference between the reflection spectra in Fig. 3 *a* and *b* originates from the fact that plasma oscillation extinction is far stronger in the p-type specimen than in the n-type one. To confirm or refute this assumption one should make a more profound analysis of these reflection spectra and calculate the parameter that controls plasmon oscillation extinction. This requires a special study and is beyond the scope of this work.

We will now dwell upon the experimental results. Table 2 shows electrical and optical measurement data and calculated b and μ_{p_h} parameters. The specimens are arranged in order of increasing ν_+ and hence increasing p_h.

The random relative errors of the parameters measured with the confidence probability $P = 0.95$ are not greater than (according to earlier special metrological studies):

– ±3 % for the electrical resistivity;

– ±6 % for the Hall coefficient;

– ≤ ±0.6 % for the characteristic wavenumber (depends on spectrometer resolution, i.e., 2 cm^{-1}, thus p_h will have the same relative error).

The absolute random error of specimen thickness measurement is half of the measurement head scale unit (0.005 mm).

As for the relative random error of the b parameter, it can be evaluated by calculation. Expressing b from Eq. (16) and assuming that this parameter is a random function of two independent variables (R_H и p_h), then, knowing the relative random errors of these parameters one can calculate the relative random error of the b parameter which proves to be not greater than ±15 % (this is an overestimate). By analogy, using Eq. (17) one can find the relative random error of μ_{p_h} to be not greater than ±20 %.

It can be seen from Table 2 that the b parameter is in the 1.9–2.8 range and there is no relation between the heavy hole concentration and the b parameter. Thus, we can state that according to our data the light to heavy hole mobility ratio proves to be quite smaller than the earlier reported values. This unexpected result requires special discussion.

The classical book by O. Madelung [15] with a reference to a work by H. Ehrenreich [16] states that scattering at optical phonons (it is accepted that this scattering type is predominant in the material in question near room temperature) cannot be described with the free carrier relaxation time by quasi-momentum. In this case the carrier mobility proves to be inversely proportional to its effective mass to a power of 3/2: $\mu \sim m^{-3/2}$. Since it is admitted that the scattering mechanisms is the same for the light and heavy holes (scattering at optical phonons), the carrier mobility ratio should be inversely proportional to the effective carrier mass ratio to a power of 3.2, i.e., $b = (\mu_{p_h}/\mu_{p_l})^{3/2} = 15.51$ (see above). However, our data show that $1.9 \le b \le 2.8$ (see Table 2).

Noteworthy, earlier works on the electrical properties of p-GaAs (see e.g. [17, 18]) did not take into account the second valence subband which is obviously incorrect.

The same is true for some later works [19–22] where the authors did not even mention the light hole subband. Interestingly, some of these authors [19, 20] initially ignored the second valence subband but later on attempted to do that [23, 24], referring to theoretical results presented in another work [25].

The authors of that work [25] attempted to take into account the effect of the light hole subband by introducing some “effective Hall factor” which is a fitting parameter that may significantly differ from unity. This parameter is determined by fitting theoretical data to experimental temperature functions of Hall coefficient and electrical resistivity. Similar calculations were carried out [26] for GaSb the valence band of which also consists of two subbands.

It was also approved [27] that the abovementioned “effective Hall factor” may vary in the 1.9–4.7 range, other researchers [28] reported a range of 1.2–2.2, and the value 2.66 was reported elsewhere [25]. This latter estimate was used [23, 24] for analysis of Hall measurement results for manganese-doped epitaxial gallium arsenide layers.

The introduction of the “effective Hall factor” formally simplifies experimental data processing, but the physical sense of this parameter remains unclear. As for the b parameter, it is generally out of research interest, it being *a priori* assumed that this parameter is the inverse efficient carrier mass ratio to a power of 3/2 (see above). Then the b parameter should be 8.57 based on earlier data [25], and 15.51 judging from our results (see above).

Our results confront the literary accepted model according to which light and heavy holes are scattered similarly (at optical phonons). Since the b parameter proved to be 5–6 times smaller than expected, it has to be admitted that the accepted model does not work. In other words, light and the heavy holes should are scattered in different ways. The available data do not allow to judge on how they scattered, and this is to be investigated in separate work.

5. Conclusion

The plasmon scattering frequency and high-frequency combined plasmon-phonon mode frequency were theoretically calculated as a function of heavy hole concentration for p-GaAs at $T = 295$ K. A calibration curve for heavy hole concentration as a function of characteristic wavenumber ν_+ was built up (described by a second-order polynomial).

The room temperature reflection spectra of 10 zinc-doped *p*-GaAs specimens were studied. The spectral dependences of the real and imaginary parts of the complex dielectric permeability were calculated using the Kramers–Kronig relations, and the loss function was built up. The characteristic wavenumbers were determined from the positions of the loss function maxima, and the heavy hole concentrations were found from the calculated calibration curve.

Electrical measurements (Van der Pau method) were carried out for the same specimens, and the electrical resistivity and the Hall coefficients were determined.

Comparison of the optical and electrical data allowed calculating the heavy to light hole mobility ratio and the heavy hole mobilities (this approach was used for the first time). We showed that $1.9 \leq b \leq 2.8$ which is quite smaller than the theoretically predicted figure (15.51). It was hypothesized that the light and heavy hole scattering mechanisms differ.

References

1. Belova I.M., Belov A.G., Kanevskii V.E., Lysenko A.P. Determining the concentration of free electrons in *n*-InSb from far-infrared reflectance spectra with allowance for plasmon-phonon coupling. *Semiconductors*. 2018; 52(15): 1942–1946. https://doi.org/10.1134/S1063782618150034
2. Yugova T.G., Belov A.G., Kanevskii V.E., Kladova E.I., Knyazev S.N. Comparison between optical and electrophysical data on free electron concentration in tellurium doped *n*-GaAs. *Modern Electronic Materials*. 2020; 6(3): 85–89. https://doi.org/10.3897/j.moem.6.3.64492
3. Yugova T.G., Belov A.G., Kanevskii V.E., Kladova E.I., Knyazev S.N., Parfent'eva I.B. Comparison between results of optical and electrical measurements of free electron concentration in *n*-InAs specimens. *Modern Electronic Material*. 2021; 7(3): 79–84. https://doi.org/10.3897/j.moem.7.3.76700
4. New semiconductor materials. Biology systems. Characteristics and properties. Band structure and carrier concentrationof gallium arsenide (GaAs). URL: https://www.ioffe.ru/SVA/NSM/Semicond/GaAs/index.html
5. Pozhela Yu.K. Plasma and current instabilities in semiconductors. Moscow: Nauka; 1977. 368 p. (In Russ.)
6. Askerov B.M. Kinetic effects in semiconductors. Leningrad: Nauka; 1970. 304 p. (In Russ.)
7. Varga B.B. Coupling of plasmons to polar phonons in degenerate semiconductors. *Physical Review Journals Archive*. 1965; 137(6A): A1896. https://doi.org/10.1103/PhysRev.137.A1896
8. Singwi K.S., Tosi M.P. Interaction of plasmons and optical phonons in degenerate semiconductors. *Physical Review Journals Archive*. 1966; 147(2): 658. https://doi.org/10.1103/PhysRev.147.658
9. Shkerdin G., Rabbaa S., Stiens J., Vounckx R. Influence of electron scattering on phonon-plasmon coupled modes dispersion and free electron absorption in doped GaN semiconductors at mid-IR wavelengths. *Physica Status Solidi (b)*. 2014; 251(4): 882–891. https://doi.org/10.1002/pssb.201350039
10. Ishioka K., Brixius K., Hofer U., Rustagi A., Thatcher E.M., Stanton C.J., Petec H. Dynamically coupled plasmon-phonon modes in GaP:An indirect-gap polar semiconductor. *Physical Review B*. 2015; 92(20): 205203. https://doi.org/10.1103/PhysRevB.92.205203
11. Volodin V.A., Efremov M.D., Preobrazhensky V.V. Semyagin B.R., Bolotov V.V., Sachkov V.A., Galaktionov E.A., Kretinin A.V. Investigation of phonon-plasmon interaction in GaAS/AlAs tunnel superlatticies. *Pis'ma v zhurnal eksperimental'noi i teoreticheskoi fiziki = Journal of Experimental and Theoretical Physics*. 2000; 71(11): 698–704. (In Russ.). https:/doi.org/10.1134/1.1307997
12. Mandal P.K., Chikan V. Plasmon-phonon copling in charged *n*-type CdSe quantum dots: a THz time-domain spectroscopic study. *Nano Letters*. 2007; 7(8): 2521–2528. https:/doi.org/10.1021/nl070853q
13. Trajic J., Romcevic N., Romcevic M., Nikiforov V.N. Plasmon-phonon and plasmon-two different phonon interaction in $Pb_{1-x}Mn_xTe$ mixed crystals. *Materials Research Bulletin*. 2007; 42(12): 2192–2201. https://doi.org/ 0.1016/j.materresbull.2007.01.003
14. Chudzinski P. Resonant plasmon-phonon coupling and its role in magneto-thermoelectricity in bismuth. *The European Physical Journal B*. 2015; 88(12): 344. https://doi.org/10.1140/epjb/e2015-60674-3
15. Madelung O. Physics of III-V compounds. J. Wiley; 1964. 480 p. (Russ. Transl.: Madelung O. Fizika poluprovodnikovykh soedinenii elementov III i V grupp. Moscow: Mir; 1967. 480 p.)
16. Ehrenreich H. Band structure and electron transport of GaAs. *Physical Review Journals Archive*. 1951;120(6):1951.
17. Rosi F.D., Meyerhofer D., Jensen R.V. Properties of p-type GaAs prepared by copper diffusion. *Journal of Applied Physics*. 1960; 31(6): 1105–1108. https://doi.org/10.1063/1.1735753
18. Hill D.E. Activation energy of holes in Zn-doped GaAs. *Journal of Applied Physics*. 1970; 41(4): 1815–818. https://doi.org/10.1063/1.1659109
19. Zhuravlev K.S., Terekhov A.S., Yakusheva N.A. Photoluminescence of complexes in epitaxial *p*-GaAs heavily doped with germanium. *Fizika i Tekhnika Poluprovodnikov*. 1988; 22(5): 777–779. (In Russ.)
20. Zhuravlev K.S., Chikichev S.I., Shtaske R., Yakusheva N.A. Investigation of complex formation in epitaxial heavily doped *p*-GaAs:Ge by photoluminescence method. *Fizika i Tekhnika Poluprovodnikov*. 1990; 24(9): 1645–1649. (In Russ.)
21. Komkov O.S., Pikhtin A.N., Zhilyaev Yu.V. Photoreflectance diagnostics of gallium arsenide. *Izvestiya Vysshikh Uchebnykh Zavedenii. Materialy Elektronnoi Tekhniki = Materials of Electronics Engineering*. 2011; (1): 45–48. (In Russ.)
22. Sharmin M., Choudhury S., Akhtar N., Begum T. Optical and transport propeties of *p*-type GaAs. *Journal of Bangladesh Academy of Sciences*. 2012; 36(1): 97–107. https://doi.org/10.3329/jbas.v36i1.10926

23. Zhuravlev K.S., Terekhov A.S., Yakusheva N.A. Manganese-bound recombination centers in epitaxial GaAs grown from bismuth melt. *Fizika i Tekhnika Poluprovodnikov*. 1998; 32(1): 50–56. (In Russ.)
24. Zhuravlev K.S., Shamirzaev T.S., Yakusheva N.A. Properties of manganese-doped gallium arsenide layers grown by liquid-phase epitaxy from a bismuth melt. *Semiconductors*. 1998; 32(7): 704–710.
25. Gouskov L., Bilac S., Pimentel J., Gouskov A. Fabrication and electrical properties of epitaxial layers of GaAs doped with manganese. *Solid-State Electronics*. 1977; 20: 653–656. https://doi.org/10.1016/0038-1101(77)90039-9
26. Campos M.D., Gouskov A., Pons J.C. Residual acceptors in natural GaSb and $Ga_xIn_{1-x}Sb$; their contribution to transport between 4.7 and 300 K. *Journal of Applied Physics*. 1973; 44(6): 2642–2646. https://doi.org/10.1063/1.1662627
27. Wenzel M., Irmer G., Monecke J., Siegel W. Hole mobilities and the effective Hall factor in *p*-type GaAs. *Journal of Applied Physics*. 1997; 81(12): 7810–7816. https://doi.org/10.1063/1.365391
28. Lee H.J., Look D.C. Hole transport in pure and doped GaAs. *Journal of Applied Physics*. 1983; 54(8): 4446–4452. https://doi.org/10.1063/1.332640